fib/sem examination of a high burn-up uo2 in the center of the pellet

J. Noirot, I. Zacharie-Aubrun, T. Blay

WRFPM 2017
2017 Water Reactor Fuel Performance Meeting

2017 Water Reactor Fuel Performance Meeting
September 10 (Sun) ~ 14 (Thu), 2017
Ramada Plaza Jeju • Jeju Island, Korea

FIB/SEM EXAMINATION OF A HIGH BURN-UP UO_2 IN THE CENTER OF THE PELLET

J. Noirot[1], I. Zacharie-Aubrun[1], T. Blay[1]

[1] *CEA, DEN, DEC, SA3C, F-13108 Saint-Paul-lez-Durance, France, jean.noirot@cea.fr*

ABSTRACT: *FIB/SEM examinations were conducted in the central part of a 73 GWd/t_U UO_2 fuel. They showed the formation of sub-domains within the initial grains. Most of the fission gas bubbles were found to be situated on the boundaries. Their shapes were far from spherical and far from lenticular. No interlinked bubble lattice was found. These observations enlighten previous unexplained observations. They plead for a revision of the classical description of the fission gas release mechanisms for the central part of the high burn-up UO_2. Yet, complementary detailed observations are needed to better understand the mechanisms involved.*

KEYWORDS: *FIB/SEM, UO_2, High Burn-up, fission gas bubbles, fission gas release, grain*

I. INTRODUCTION

In ref. [1] in 2004, we showed how post irradiation examinations of high burn-up LWR UO_2 were used for providing detailed validation data to fuel behavior codes [2-4]. The examinations presented in this paper were focused on fission gas behavior. They included electron probe micro-analyzer (EPMA), secondary ion mass spectrometer (SIMS), scanning electron microscope (SEM) measurements as well as annealing tests dedicated at intergranular gas retention measurements. In particular, high burn-up UO_2 polished samples were examined using a PHILIPS XL30 SEM with a W filament electron gun and a Centaurus KE developments back scattered electron (BSE) detector. The purpose of these SEM examinations was to derive, from the same images, the bubbles at the surface of the examined fields and the grain boundary lattice. This grain boundary lattice was extracted from the images, using contrasts between the UO_2 grains. These contrasts were due to differences in the electron channeling in the UO_2 crystal lattice, function of its local orientation. The result of this was that it was then possible to obtain information on inter-granular bubbles and on intra-granular bubbles separately, but in the same fields, using the same images.

However, this ref. [1] also showed that this technique could not be applied in the central area of the fuel where this kind of information was the most needed. Indeed, this central area, where the temperatures are the highest during normal operation, is the origin of a significant fraction of the fission gas release. Depending on temperature and burn-up, fission gases diffuse and form bubbles [5-6]. Part of these fission gases are released to the free volumes of the rod. The fission gas release mechanisms are related to this gas precipitation and interact with it, hence a high interest for inter-granular and intra-granular bubble characterization. Fig. 1 shows a SEM image taken at the external limit of the central precipitation area of a 61 GWd/t_U sample. This image shows, for this sample, a sharp transition around 0.54R (where R is the radius of the pellet, 0R corresponding to the center and 1R to the rim of the pellet). Beyond this limit, grain contrasts are visible, but on the central side, where a high density of quasi micrometric bubbles formed, the situation is quite unclear. Grains are partly visible, but there is no way to make the difference between inter-granular and intra-granular bubbles. In order to produce the data needed by the modelers, a two-step process was then adopted, with image acquisitions for the bubble and pore image analyses followed by a chemical etching to reveal the positions of the grain boundaries and new image acquisitions in the same fields. About the change in the electron channeling we wrote in [1] that "*This demonstrates the influence of the gas precipitation on the SEM crystallographic contrast and is to be precisely analyzed in a subsequent publication*", but we were not able to really go much further than thinking of good reasons for this change, with no experimental evidence to support these ideas.

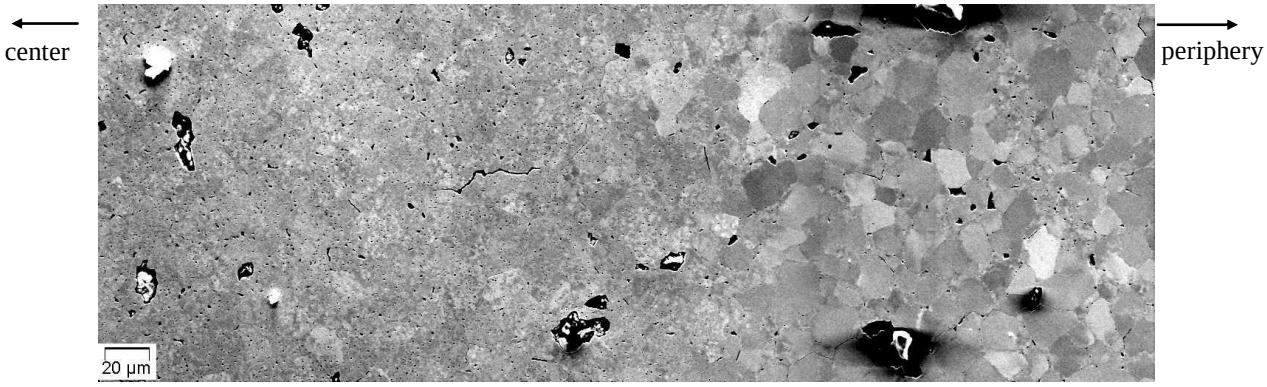

Fig. 1. Crystallographic contrast image at the limit of the central precipitation zone on a 61 GWd/t_U irradiated UO_2, from ref. [1]

In ref. [7-8] in 2008, among the presented results, there were SEM fractography images of a UO_2 sample irradiated at 73 GWd/t_U. In the center of this fuel, large bubbles were observed (Fig. 2). These bubbles were neither spherical nor clearly lenticular, and they did not seem to be widely interconnected. We then mentioned that it was not so easy to see the difference between inter- and intragranular surfaces in these fractographs, and to identify the grain boundaries.

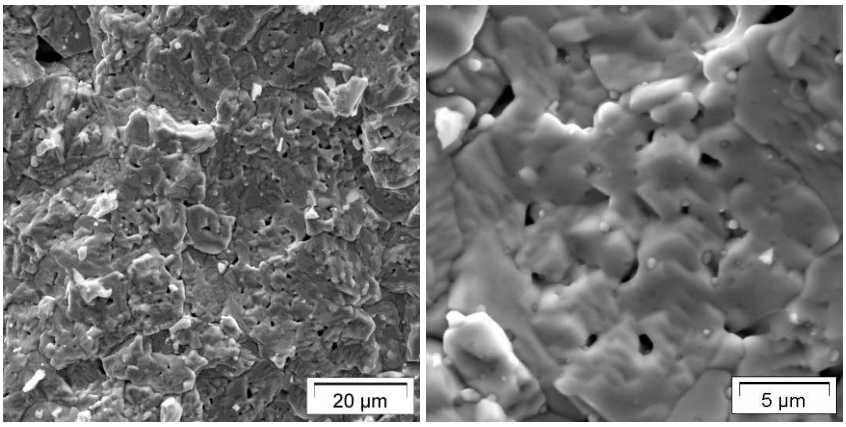

Fig. 2. SEM fractograph of a 73 GWd/t_U UO_2 sample at the center of the pellet, from [7-8]

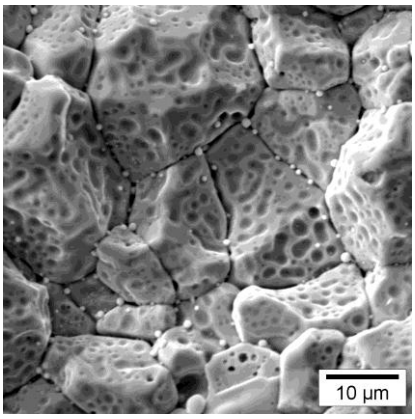

Fig. 3. SEM fractograph in the center of a 38.8 GWd/t_U PWR UO_2 fuel after an unfailed ramp test. The maximum linear power, 520 W.cm^{-1} was held for 90 s, from [9]

In the classical representation of the fission gas release process, during normal fuel operation, in the hot central parts:

- intra-granular gas diffusion leads to a build-up of fission gases accumulating in inter-granular position.
- these fission gases form intergranular bubbles.
- these intergranular bubbles interconnect, eventually forming tunnel mazes that are paths for the release of the fission gases to the free volumes of the rods [10 (p.318)] and [11-12].

The absence of such clearly visible tunnels in the fuels presented in [1, 7-8] in spite of significant fission gas release was a disturbing point in these observations.

In fact in our own experience, such tunnel mazes were observed after ramp tests (Fig. 3) and after out-of-pile annealing tests [9, 13-14]. In the literature, in addition to similar situations [15-19] such maze like tunnel structures were observed in high linear power irradiations, or in experimental irradiations for which the temperature levels in the fuel were set to high levels.

In the fuels presented in [1, 7-8] the burn-ups were high but the rod average linear powers had never reached values higher than 203 W.cm^{-1} and the fuel behavior code calculations showed that the fuel centerline temperatures were in the range

800-900 °C during the last three cycles for the rods examined at 83 GWd/t_U, after 7 cycles of irradiation. Nonetheless, in spite of moderate central temperatures and in spite of no obvious intergranular bubble interlinkage, fission gas release rates clearly increased at high burn-up.

In 2016, we replaced our PHILIPS XL30 SEM by a FIB/SEM with improved performances and extra capacities. We used it to address some of the questions remaining after these first examination series.

II. Experimentals

II.A. Examined fuel basic data

The fuel examined in this paper was a UO_2 fuel with an initial ^{235}U enrichment of 4.5%.
It had an initial porosity around 5%. The initial grains sizes were around 11 µm. The resintering tests led to 0.4% of densification after one day at 1700 °C, 0.61% after two days, and 0.7% after four days. The cladding was M5®. It was irradiated six annual cycles in the EDF Gravelines 5 reactor. The mean rod burnup was 67.5 GWd/t_U.
Fig. 4 gives, for the examined rod, a simplified history of the average linear power. The highest mean linear powers, around 200 W.cm^{-1}, were during the first cycle. The second cycle linear powers were low. During the three last cycles the average linear powers were below 188 W.cm^{-1}.
The rod puncturing fission gas release rate was 6.2%. For this program, it was the highest among the rods punctured after six annual irradiation cycles (solid mark in Fig. 5).
The sample examined was taken at 793 mm from the rod bottom, in the second span, and had an average section burn-up of 73 GWd/t_U.

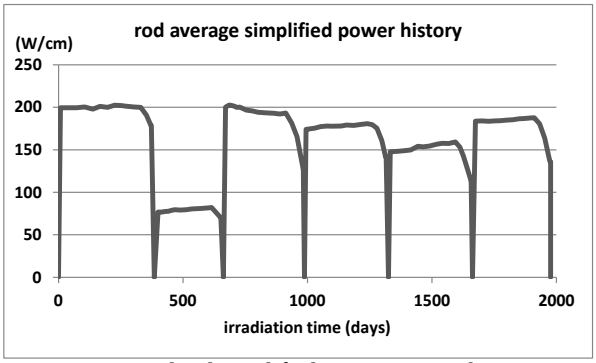

Fig. 4. Examined rod simplified average power history

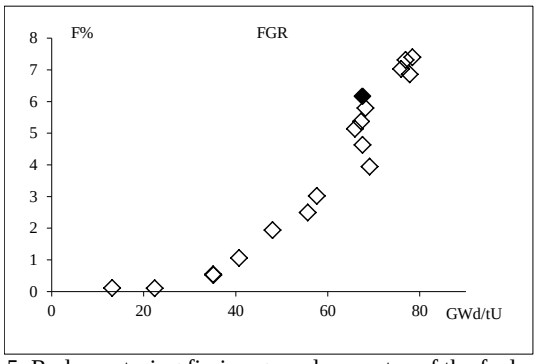

Fig. 5. Rod puncturing fission gas release rates of the fuels presented in [7-8]. The solid mark corresponds to the rod on which extra examinations are presented in this paper

II.A. Experimental device used

The new FIB/SEM installed in our CEA Cadarache LECA-STAR hot-cell facility is in a shielded cell and connected to a glove box in order to prevent contamination [20-21]. It is a field emission electron gun Carl Zeiss Auriga 40.
It is equipped with:

- A secondary electrons secondary ion detector (SESI), a Crytur YAG crystal based scintillator back scattered electron detector, secondary electrons (SE) and energy selective backscattered (ESB) inlens detectors.
- An Orsay Physics COBRA focused ion beam (FIB) column.
- An Oxford energy dispersive spectroscopy (EDS) detector.
- An Oxford electron back scattered diffraction (EBSD) detector.
- An Anton-Paar nano-indenter and a Kleindick micro-manipulator that can both be mounted on the door of the SEM chamber.
- A Zeiss scanning transmission electron microscopy (STEM) installed on the stage.

Depending on the study at hand, some of the needed accessories have to be positioned and connected manually via the gloves before introducing the radioactive sample in the SEM chamber.
The EDX and the STEM detectors must only be used on micro-samples with very low irradiation levels, to avoid gamma damage to the sensitive parts of the detectors.
The work presented in this paper, mainly involved the FIB and the electron detectors.

In these 3D FIB/SEM examinations, a polished cross section of irradiated fuel is tilted in the SEM chamber, so that its plane polished surface is perpendicular to the direction of the Ga ion beam. This ion beam direction forms a 54° angle with the vertical electron beam of the SEM. The FIB is used for nano-machining the specimen. After creating an empty space in front of the surface that will be examined, slices are machined, step by step. Between each step, using the electron beam and the electron detectors, an image of each slice surface is taken. The series of these images in which the pixel sizes are similar to the thickness of the slices, brings local 3D information on the fuel microstructure.

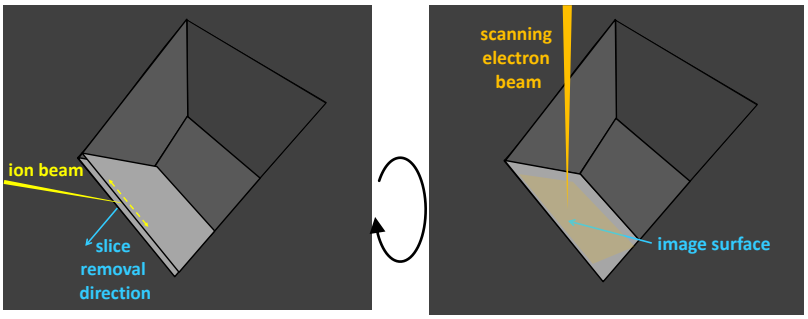

Fig. 6. 3D FIB/SEM examination principle

III. FIB/SEM 3D examination

Fig. 7 shows the tenth image of a FIB/SEM sequence of 270 images. This FIB/SEM work was conducted close to the center of the radial cut of the 73 GWd/t_U sample. The field covered by this image is 26×10 µm^2 with pixels of 17×17 nm^2. The distance between each examined surface, i.e. the thickness of the slices cut by the FIB, is the same as the pixel size: 17 nm. The total thickness explored with these images corresponds to 4.6 µm, for a total fuel volume close to 1200 µm^3.

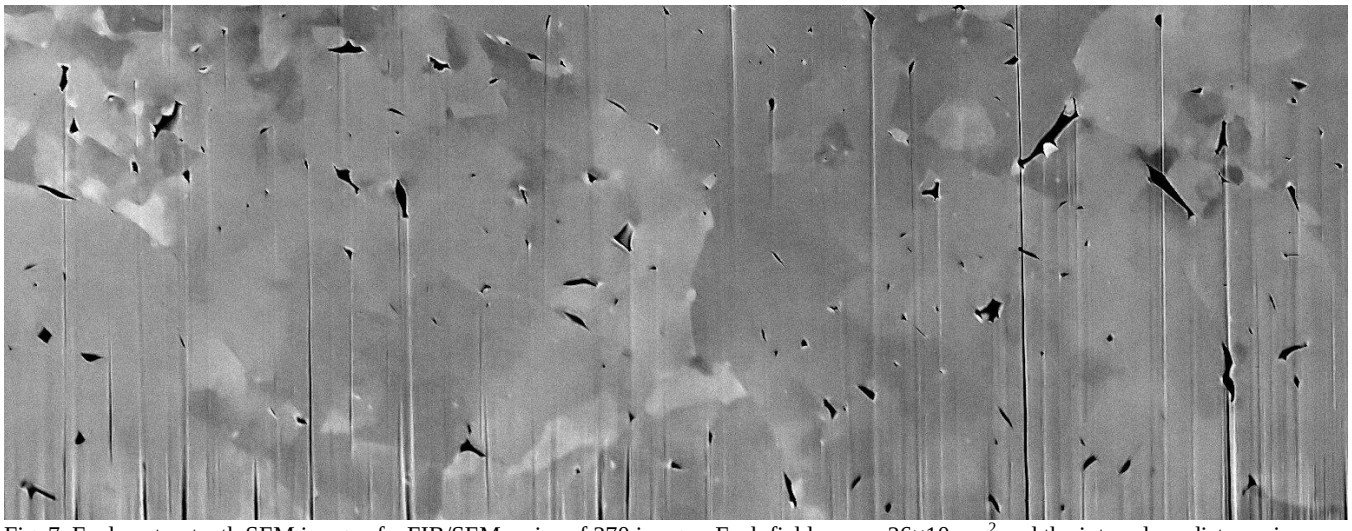
Fig. 7. Fuel center, tenth SEM image of a FIB/SEM series of 270 images. Each field covers 26×10 µm^2 and the inter-plane distance is 17 nm. The whole series covers a thickness of 4.6 µm

Fig. 8 shows, as examples, 8 of these 270 images, one out of 33 of the images of this series. The distance between each shown plane is 0.56 µm. These images read from left to right and from top to bottom, so that the first image is at the top left of the figure and the last one at the bottom right. This will be the case for all image series presented here. The image presented in Fig. 7 is situated between the first two images of Fig. 8. In the post-treatment of these images, an alignment was necessary, to rectify scanning shifts, partly due to the observation plane displacement.
In these images, the vertical lines are due to the influence of the bubbles on the Ga ion beam micro-machining of the samples. This unwanted artefact, called "curtaining" effect is difficult to fully avoid. It is particularly visible in these images because their contrast was enhanced. The contrast was enhanced in order to better see the electron channeling effect, the same as in Fig. 1.
With SEM images covering fields of 26×10 µm^2 and fuel initial grain size around 11 µm, only a few grains are expected in these images. In spite of this, a large number of typically 1 µm wide areas exhibit grey level differences with their neighborhood and the initial grain boundaries do not appear clearly, even if they can be partly guessed thanks to the largest bubbles and pores. These areas with grey level differences show the existence, in the central part of this fuel, of domains with crystal orientation differences with that of their original grain. These SEM channeling images give no information on the disorientation degree of these domains, compared to that of the original grain.
Fig. 9 gives a detailed series of 30 images, restricting the area to 4.15×3.38 µm^2, with inter-plane distances of 0.051 µm, i.e. one image out of three acquired images, over a thickness of 1.4 µm, inside an initial grain.

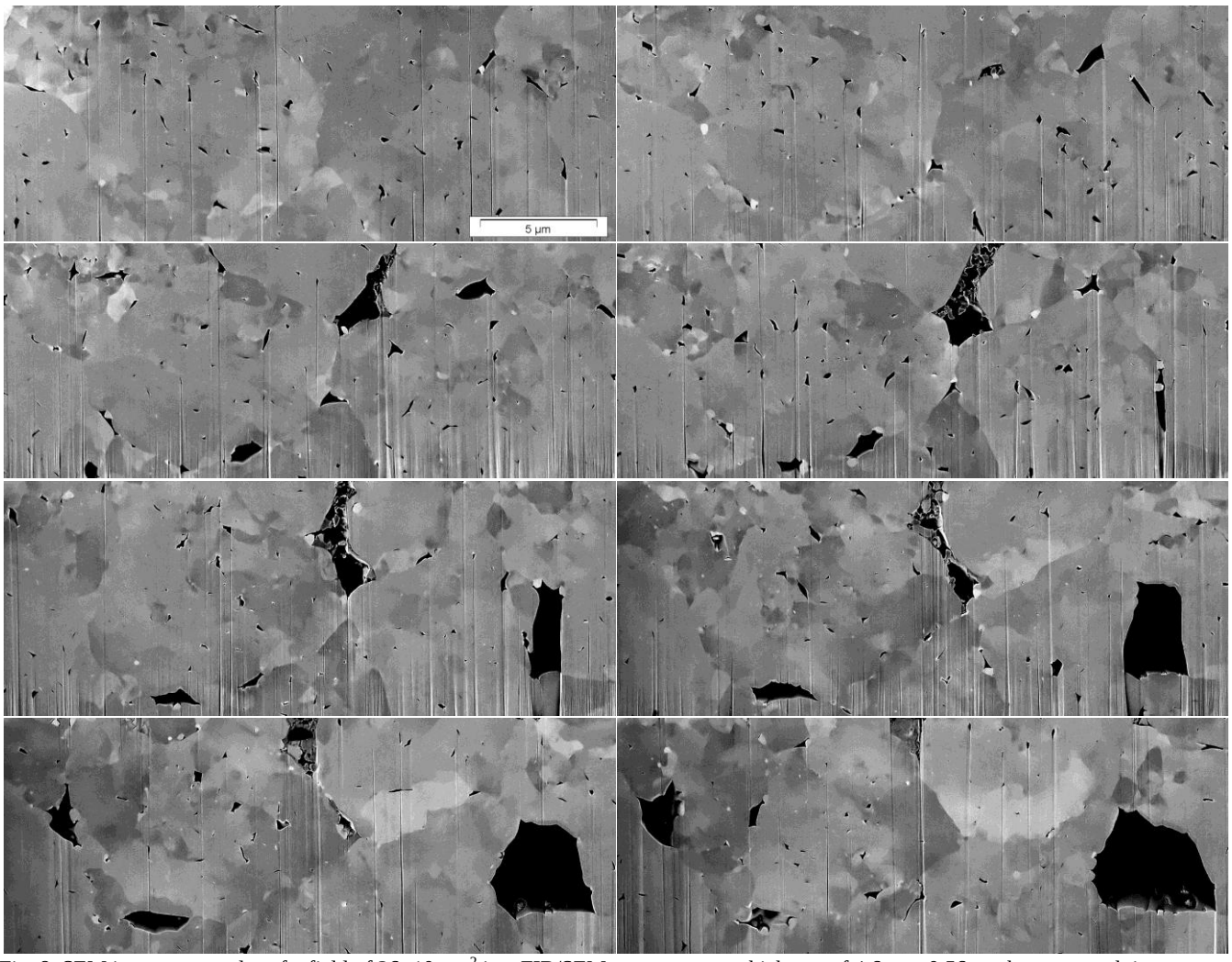

Fig. 8. SEM images examples of a field of 26×10 µm^2 in a FIB/SEM sequence over thickness of 4.6 µm. 0.56 µm between each image

A striking point is that almost all the bubbles appear to be situated along borders between these domains. The largest bubbles or pores are probably along the initial grain boundaries, but some of the "intra-granular" "inter-domain" bubbles can be quite large. No interconnections between the bubbles were found. Three of these large inter-domain bubbles, labelled 1, 2 and 3 in the images presented in Fig. 9 have been extracted to be presented, as seen from four directions, Fig. 10. The shape of the large bubbles can be quite complicated as in can be seen with these examples. Their respective volumes were 0.120 μm^3, 0.053 μm^3 and 0.019 μm^3. Spheres with the same volumes would have diameters of 0.61 µm, 0.47 µm and 0.33 µm.

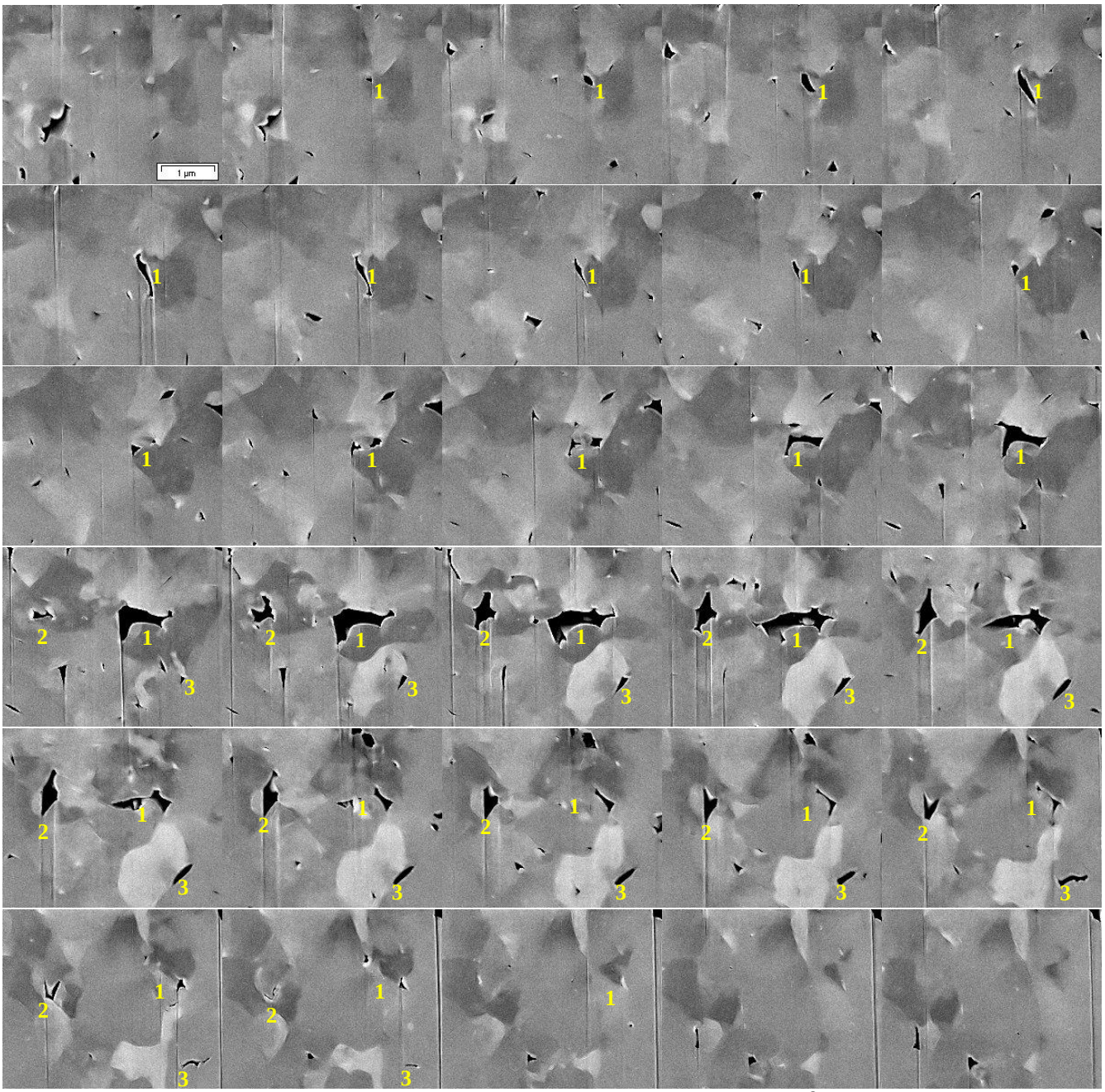

Fig. 9. Fuel center, details from the same sequence as that of Fig. 7 and Fig. 8. Fields of 4.15×3.38 μm^2, with inter-plane distances o51 nm i.e. one image out of three. These images cover a thickness of 1.4 µm. Labels 1, 2 and 3 follow the bubbles visualized Fig. 10

Much smaller inter-domain bubbles were also found. Four examples are visible in Fig. 10 in addition to bubbles labelled 2 and 3. No interconnections between these smaller bubbles were visible either.
In these images, in addition to the bubbles and the domain grey level contrasts, metallic fission products were detected. They form the brightest spots. Most of them appear to be situated in inter-granular, in inter-domain position or at the surface of large bubbles or pores. They are most of the time associated with a cavity, but this cavity can be much smaller than them. At the surface of the large pores, most of these metallic fission products precipitates are situated at the emerging domain boundaries (Fig. 11). These emerging boundaries clearly appear as dark furrows, like grain boundaries. The metallic fission products appear to have, there, raspberry-like surfaces.

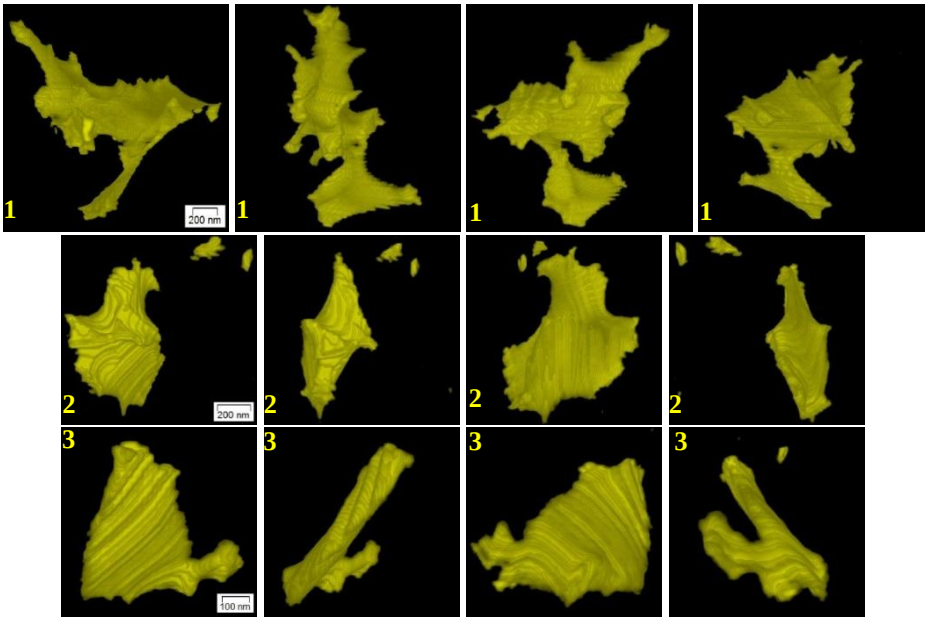

Fig. 10. Four views of the bubbles labeled 1, 2 and 3 in Fig. 9

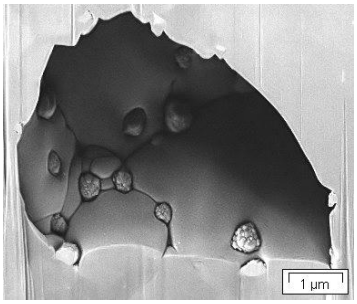

Fig. 11. SEM view inside the large pore visible at the end of Fig. 8 sequence

Fig. 12 shows another example of images taken from a series of 148 images from the same sample, but at 0.36R, i.e. for this fuel in the peripheral part of the central gas precipitation area. These fields cover a surface of 23.2×10.5 µm^2 with 15 nm pixels and inter-plane distances of 15 nm. The whole series covers a thickness of 2.2 µm. In these examples, the distance between the images is 0.44 µm.

Fig. 13 shows an extract from the same sequence as Fig. 12, over a bloc of 2.6×3×1.4 µm^3, with inter-image distances of 45 nm, one image out of three.

As in the center of the pellet, at this radial position, domains with crystal orientations differences with that of the original grains, are evidenced. Also, at this radial position, most of the bubbles and pores are observed in inter-granular or inter-domain position. The bubble shapes are also far from spherical, lenticular and they are not connected to the free volumes outside the pellets. The shape of the largest inter-domain bubble from the extract Fig. 13 is shown in Fig. 14. The volume of this bubble was 0.38 µm^3 (a sphere with the same volume would have a diameter of 0.9 µm). The grain/domain surfaces at the interface with the bubble are convex.

The main difference with the previous observations, closer to the center, is the detection of smaller metallic fission product precipitates (bright dots in the images). Some of these precipitates may not be in inter-domain position.

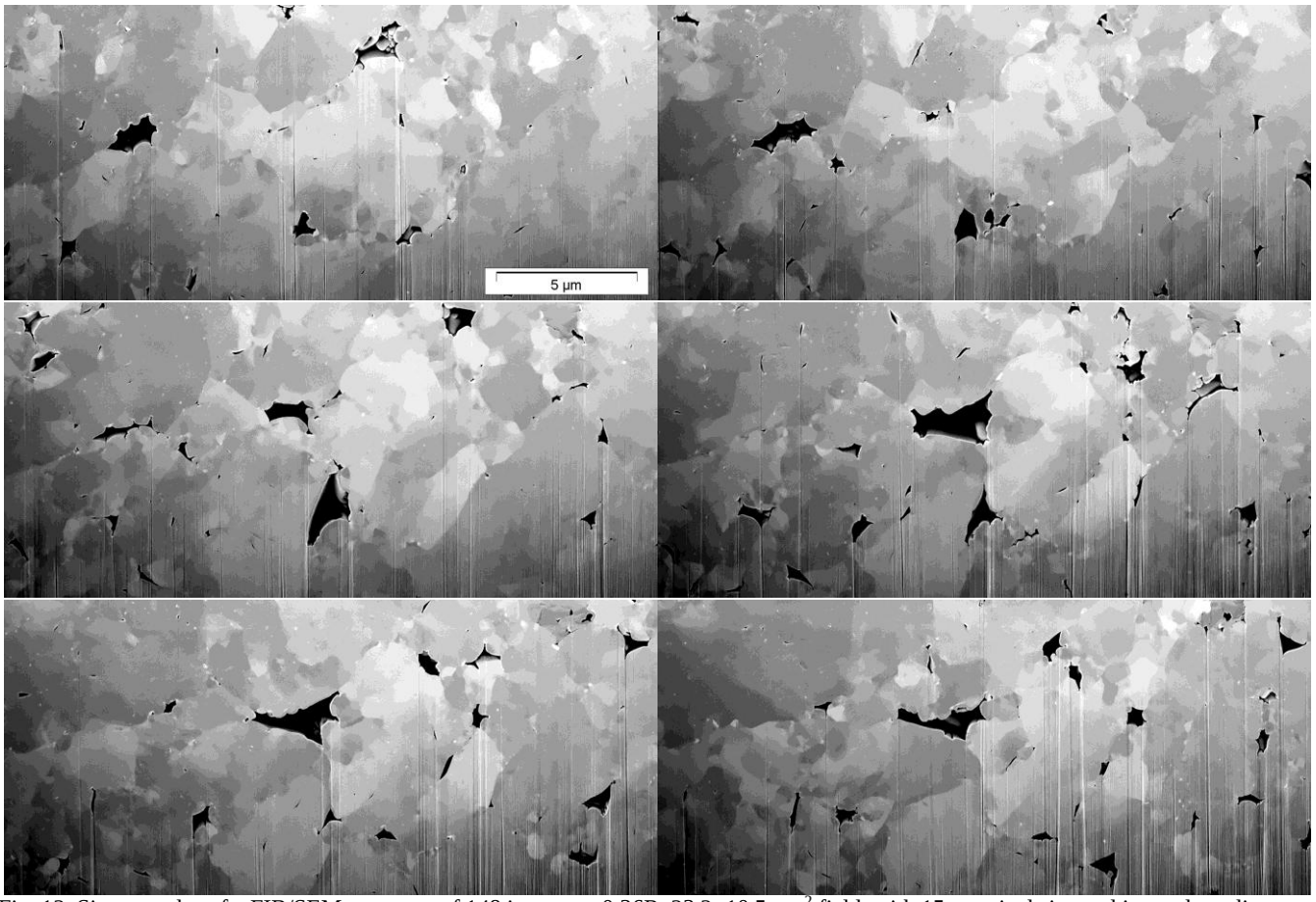

Fig. 12. Six examples of a FIB/SEM sequence of 148 images at 0.36R. 23.2×10.5 µm^2 field, with 15 nm pixel size and inter-plane distances

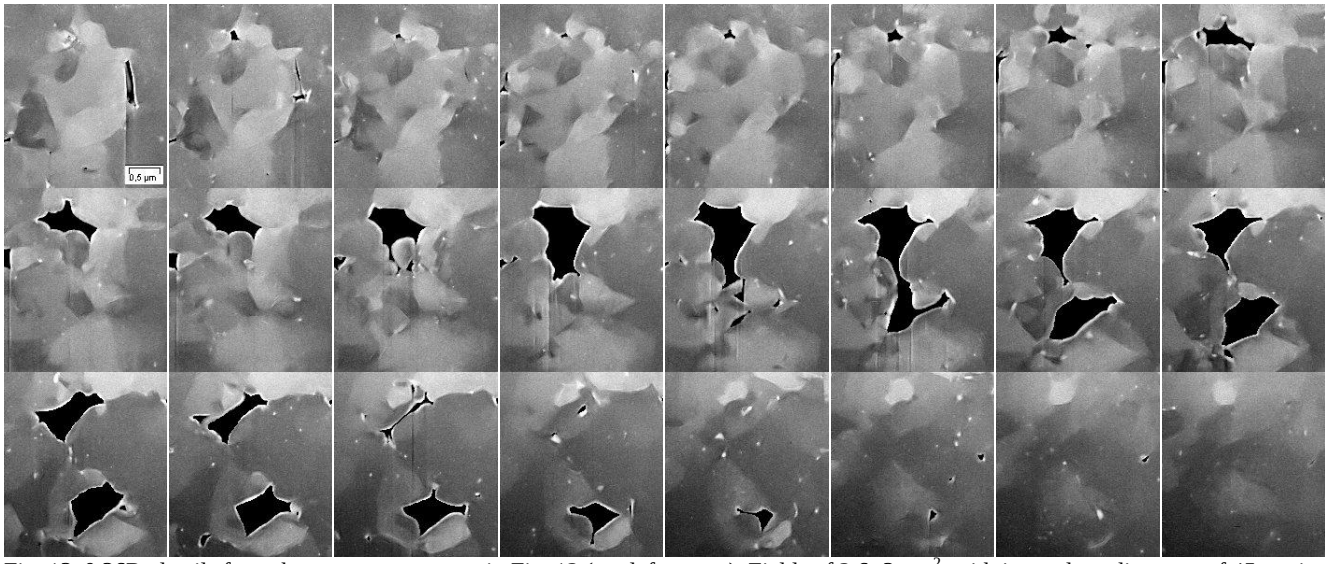

Fig. 13. 0.36R, details from the same sequence as in Fig. 12 (top left corner). Fields of 2.6×3 µm^2, with inter-plane distances of 45 nm i.e. one image out of three. This extract covers a thickness of ~1.4 µm.

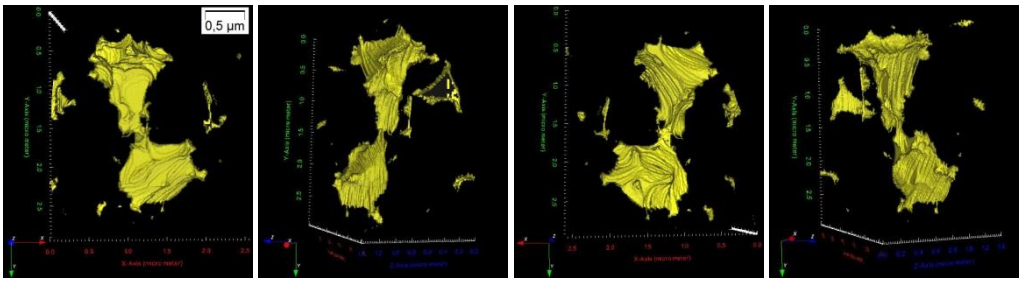

Fig. 14. 0.36R, four views of the bubbles in the volume corresponding to Fig. 13

IV. DISCUSSION-CONCLUSION

FIB/SEM examinations in the central part of a high burn-up UO_2 fuel have shown the formation of sub-domains within the initial grains. They also showed the presence of inter-domain bubbles and the absence of interconnected bubble lattice. These bubbles are far from spherical and often far from lenticular.

With these FIB/SEM examinations, the questions raised by the observations like those presented in Fig. 1 and Fig. 2 find a partial answer:

- The lower magnification SEM images of the polished sample could not exhibit the same grain contrasts in the central parts of the pellets as outside this central part because within the grains many sub-domains, with different crystal orientations had formed.
- The inter-granular or trans-granular nature of the fractograph central surfaces was difficult to determine because part of it corresponded to fractures of the boundaries between these domains.
- No obvious interconnected inter-granular bubble lattice was observed on polished samples or on fractographs because it does not form with these irradiation conditions. Neither on the initial grain boundaries, nor on the boundaries between the new domains.

These observations also bring some explanation to the microstructure of fragments formed during a 20°C.s^{-1} annealing test at 1200°C on a 83 GWd/t_U UO_2 fuel during which, in all areas with a high density of fission gas bubbles, fragmentation occurred, including in the central part. Indeed, the fragments formed in the central part of the pellet seemed surprisingly not to correspond to intergranular fragmentation [22].
Moreover, these observations are quite consistent with results brought by the synchrotron work conducted by the Paul Sherrer Institut using the Swiss Light Source synchrotron, showing sub-grain formation in high burn-up fuel central areas [23-24].

Nonetheless, new questions are raised from these observations:

- What are the mechanisms leading to the formation of these domains?
- What are the mechanisms leading to the inter-granular and inter-domain bubbles and to their morphology?
- And above all, what are the mechanisms leading to an increase of fission gas release at high burn-up, without the activation of the inter-granular bubble interconnection phenomenon?

The formation of a higher density of boundaries in the central part of the fuel probably participates to the explanations of the fission gas release increasing rate at high burn-up. However, the detailed mechanisms involved are still to be found.
At the Imperial College (UK) Molecular Dynamic calculations were used in [25] to study Xe diffusion and bubble nucleation around edge dislocations in UO_2. This study concluded that fast diffusion of Xe along the dislocation core was inhibited by Xe clustering in nano-bubbles along these dislocations. At CEA, ref. [26] showed the influence of the presence of a grain boundary on the atom displacements in a fission product recoil cascade. Work should be done in this field to evaluate the influence of grain boundaries and of these domain boundaries on the fission gas movements in the fuel.

EBSD characterizations of the new microstructure are ongoing, using the same FIB/SEM. They will give the local crystal orientations in the various domains.
Detailed TEM characterizations are planned. They are necessary to try to understand the formation mechanisms of this new microstructure and to try to progress on this matter.

ACKNOWLEDGMENTS

The authors are thankful to EDF and AREVA for their support in the studies using these irradiated fuels that they made and used in nuclear power plants.

In addition to the FIB/SEM software, analySIS, FIJI and Icy have been used for image processing and analyses.

REFERENCES

1. J. NOIROT, ET AL., *Fission Gas Inventory in PWR High Burnup Fuel : Experimental Characterization and Modeling* ANS LWR Fuel Performance, Orlando, Florida (USA), (2004).
2. L. NOIROT, Journal of Nuclear Science and Technology *43*, pp 1149-1160, (2006).
3. L. NOIROT, Nuclear Engineering and Design *241*, pp 2099-2118, (2011).
4. V. MARELLE, ET AL., *New developments in ALCYONE 2.0 fuel performance code*, TOPFUEL, Boise, Idaho (USA), (2016).
5. P. GUEDENEY, ET AL., *Standard PWR fuel rod characterization at high burn-up*, International topical meeting on LWR fuel performance, Avignon (France), (1991).
6. R. MANZEL, ET AL., Journal of Nuclear Materials *301*, pp 170-182, (2002).
7. J. NOIROT, ET AL., Nuclear Engineering and Technology *41*, pp 155-162, (2009).
8. J. NOIROT, ET AL., *High burnup changes in UO2 fuels irradiated up to 83 GWd/t in M5® claddings*, WRFPM, Seoul (South Korea), paper 8036, (2008).
9. J. NOIROT, ET AL., *LWR fuel gas characterization at CEA Cadarache LECA-STAR Hot Laboratory*, IAEA-TECDOC-CD-1635, (2009).
10. D.R. OLANDER, *Fundamental aspects of nuclear reactor fuel elements*, (1976).
11. J.R. MATTHEWS, ET AL., Eur. Appt. Res. Rept.- Nucl. Sci. Technol. *5*, (1984).
12. D. BARON, ET AL., *Fuel Performance of Light Water Reactors (Uranium Oxide and MOX)*, *Comprehensive Nuclear Materials*, Elsevier, (2012).
13. I. ZACHARIE, ET AL., Journal of Nuclear Materials *255*, pp 92-104, (1998).
14. S. VALIN, ET AL., *Modelling the behaviour of intergranular fission gas during out-of-pile annealing*, Fission Gas Behaviour in Water Reactor Fuels, Cadarache (France), pp 357-368, (2000).
15. J.A. TURNBULL, ET AL., Philosophical Magazine *30:1*, pp 47-63, (1974).
16. C. BAKER, ET AL., *Fission gas release during post irradiation annealing of UO2*, Int. Conf. on Materials for Nuclear Reactor Core Applications, BNES Bristol (UK), (1987).
17. R.J. WHITE, Journal of Nuclear Materials *325*, pp 61-77, (2004).
18. P. COOK, ET AL., *Post-Irradiation Examination and Testing of BNFL SBR MOX Fuel*, Proceedings of the 2004 International Meeting on LWR Fuel Performance, Orlando, Florida (USA), Paper 1015, (2004).
19. M.A. BARKER, ET AL., *Experimental and Computational Analysis of the Development of Intergranular Bubbles in Oxide Fuels*, TOP-FUEL, Paris (France), (2009).
20. I. ZACHARIE-AUBRUN, ET AL., *A new look on irradiated fuels at the CEA Cadarache*, NuMat, Montpellier, (France), (2016).
21. I. ZACHARIE-AUBRUN, ET AL., *New capabilities of analyses with a versatile nuclearized dual beam*, Hotlab, Karlsruhe (Germany), (2016).
22. J. NOIROT, ET AL., *Size and radial origin of fragments formed while heating a 83 GWd/tU PWR fuel up to 1200 °C*, LOCA Workshop, Fuel fragmentation, relocation and dispersal (FFRD) – experimental basis, mechanisms and modelling approaches, Aix-en-Provence (France), (2015).
23. M. CHOLLET, ET AL., *Synchrotron XRD Analysis of Irradiated UO2 Fuel at Various Burn-up*, TopFuel, Boise, Idaho (USA), (2016).
24. M. CHOLLET, ET AL., *From Fresh to 9-cycle UO2 Fuel: Microstructure Evolution Studied by Synchrotron X-ray Diffraction*, WRFPM, Jeju (Korea), (2017).
25. S.T. MURPHY, ET AL., Journal of Nuclear Materials *466*, pp 634-637, (2015).
26. L.V. BRUTZEL, ET AL., Journal of Nuclear Materials *377*, pp 522-527, (2008).